Microscopic Dimensions Engineering: Stepwise Manipulation of the Surface Wettability on 3D Substrates for Oil/Water Separation

*Ran Du, Xin Gao, Qingliang Feng, Qiuchen Zhao, Pan Li, Shibin Deng, Liurong Shi, and Jin Zhang**

In recent years, research on fabricating superwettable materials, especially superhydrophobic materials, has received wide attention for their diverse applications ranging from self-cleaning coatings, water remediation to energy-related fields.[1–10] To achieve superhydrophobicity, two requirements need to be met: a low energy surface (to provide high water contact angle (CA) on flat surfaces) and a high surface roughness (to amplify the intrinsic hydrophobicity). Since nearly all flat surfaces cannot display sufficient hydrophobicity with only low-energy coatings,[1,11] controlled fabrication of microstructures is of paramount importance to modulate the surface roughness and thus realizing superhydrophobicity. However, until now it is still quite challenging to fabricate well-defined microstructures, especially on three-dimensional substrates, for achieving controllable surface roughness and wettability, thereby hindering the design and fabrication of superior bulk superhydrophobic materials.

Typically, superhydrophobic materials are fabricated by either constructing microstructures on as-existed two-dimensional (2D)/three dimensional (3D) substrates, or by one-step bottom-up assembly process. In last few decades, significant advances have been achieved in fabricating superhydrophobic 2D substrate (e.g., silicon wafers, stainless steel meshes), versatile well-defined structures have been created.[12–20] For example, Jiang's group has made striking progress in synthesizing well-defined zero-dimensional (0D), one-dimensional (1D), and other specific microstructures on flat surfaces by using polymers or aligned carbon nanotubes (ACNTs).[13,14] They have also showed the superwettability can be switched by utilizing microstructures with stimuli-responsive nature.[21] In addition, the same group have proposed the micro/nano two-level design principle for microstructures fabrication, so as to achieve extraordinary water repellence.[22,23] However, few efforts have been dedicated to scientifically and systematically modulating the surface roughness (R_f), thus hampering the intentional design of superior superwettable materials. Moreover, the 2D substrate is very thin, which means it possesses fewer hydrophobic surfaces and small volume. Hence, it is hard to acquire high processing capacity for water remediation such as oil uptake and oil/water separation.[15,24] Therefore, from the view of industrial applications, the 3D superhydrophobic substrate (3D-SS) is a better choice.

To design and fabricate superior 3D-SS, the precise control of microstructures over the whole 3D substrate is crucial. Unfortunately, due to the complex 3D structures, traditional methods used in the 2D substrate for precise microstructure control, e.g., lithography, nanoimprint pattern transfer, strain-induced wrinkling, robot punching, etc.,[12,17,20,25,26] are hard to apply to its 3D counterpart. The current methods used for 3D substrates preparation can be mainly divided into two types. In first type, substrates are directly constructed by bottom-up assembly, e.g., carbon-based aerogels[27–34] and microporous polymer aerogels.[35,36] Recently, Yu's group has fabricated hydrophobic aerogels by using either 1D carbonaceous fibers[32,33] or 2D graphene sheets[34] as the building blocks. However, this one-step method is difficult to simultaneously control structures on both micro-level and nano-level. Additionally, the effect of dimensions of building blocks on the surface roughness and the hydrophobicity have not been studied. In another type, the as-obtained 3D networks with as-existed micro-level structures, e.g., commercial sponges,[37–43] copper foams[24] are used as supports. Nano-level structures are then introduced by post-modification. Nevertheless, during the modification process, the lack of effective control of the reaction kinetics often results into disordered microstructures. Therefore, though some works achieved high water CA on 3D substrates,[37,42] the better control of microstructure is strongly needed to promote the understanding toward 3D-SS and benefit the design of new materials. Recently, certain efforts have been done to address these problems. For example, Yu's group has created superhydrophobic surfaces (composed by clear 1D nanostructures) on versatile substrates by templating microstructured hydrogel matrix.[44] Liu's group prepared vertically aligned honeycomb-like microstructures with extraordinary superhydrophobicity based on graphdiyne.[45] However, both works can produce only one kind

R. Du, X. Gao, Q. L. Feng, Q. C. Zhao, P. Li, Dr. S. B. Deng, L. R. Shi, Prof. J. Zhang
Center for Nanochemistry
Beijing National Laboratory for Molecular Sciences
Key Laboratory for the Physics and Chemistry of Nanodevices
State Key Laboratory for Structural Chemistry of Unstable and Stable Species
College of Chemistry and Molecular Engineering
Peking University
Beijing 100871, P. R. China
E-mail: jinzhang@pku.edu.cn
Q. L. Feng
School of Chemistry and Chemical Engineering
Lanzhou University
Lanzhou 730000, P. R. China

DOI: 10.1002/adma.201504542

of microstructure, failing to provide a chance to summarize a general rule in designing good 3D-SS systems.

In this regard, we hypothesize that the rational selection and combination of microstructures with different dimensions can manipulate the surface roughness of the 3D substrate in a controllable manner. For microstructures with the single-type dimension, the R_f is determined by the dimension's type. Whereas, for microstructures with two type dimensions, the surface roughness is determined by the joint contribution of each dimension, i.e., $R_a = f(R_1, R_2)$, where R_a, R_1, and R_2 represent the apparent roughness, the roughness contributed by the first dimension and the second dimension, respectively. Thus, by manipulating the dimension types and elaborately combining them together, the surface roughness can be effectively modulated and expanded in a controllable manner (**Figure 1**). To this end, by engineering dimensions of microstructures (defined as microscopic dimensions) on 3D substrate, we can not only provide a new perspective for stepwise modulation of hydrophobicity but also extract useful rules for 3D-SS design with the assistance of theoretically modeling. Herein, we have fabricated a series of microstructures with well-defined dimensions including 0D, 1D, 2D, 0D and 1D, and 1D and 2D on commercial melamine foams (MF) through the combination of wet and dry chemistry. By carrying out extensive experiments and theoretical modeling, the relationship between microscopic dimensions (surface roughness) and the wettability (represented by static contact angle, sliding angle, and contact angle hysteresis) has been established, certain guidelines for materials design have been revealed. Additionally, we also demonstrated the power of microscopic dimensions design for oil/water separation and selective oil adsorption.

The general fabrication process is schemed in **Figure 2**a. Commercial MF was used as the 3D substrate due to its low density, porous structure, and good thermal stability (Figure S1, Supporting Information). Carbon nanotubes (CNTs), cobalt and its salts were used to construct the specific microstructures. The MF were first modified with microstructures with different dimensions by the combination of wet and dry chemistry including dipping, controlled precipitation, ice-mediated coating, and annealing process, finally generating hierarchical-dimensional melamine foam (HD-MF). It should be noted that the appropriate selection of loading methods and materials is quite important. For example, ice-mediated coating is capable of forcing materials to deposit on surfaces of 3D networks by continuously ice growth during freezing.[46] Reaction kinetics control of the cobalt salts precipitation is essential to generate regular microstructures.[47] The low decomposition temperature of cobalt acetate and the low free energy change for further reduction reaction[48,49] allow the successfully cobalt loading under moderate annealing temperature in reducing environment. Considering all factors mentioned above, diverse microstructures with different microscopic dimensions can be fabricated by selection and optimization of reaction conditions. More details can be found in the Supporting Information.

As shown in Figure 2b–g and Figures S2 and S3 (Supporting Information), microstructures with different single dimension (0D, 1D, 2D) or dimension combinations (0/1D, 1/2D) were successfully fabricated on 3D MF. For simplicity, the resultant MF are denoted as MF-*X*D, where the *X* represents the microscopic dimensions. For MF with single-type microscopic dimension, MF-0D is covered by a monolayer of uniform 0D cobalt nanoparticles (Figures S4–S6, Supporting Information), MF-1D is covered by randomly distributed 1D CNTs, and MF-2D is covered by vertically aligned 2D cobalt(II) hydroxide sheets (Figures S4 and S5, Supporting Information). The morphology of microstructures on MF-0D and MF-2D is favored for establishing theoretical model because of their relative uniform distribution or appropriate configuration, which is difficult to

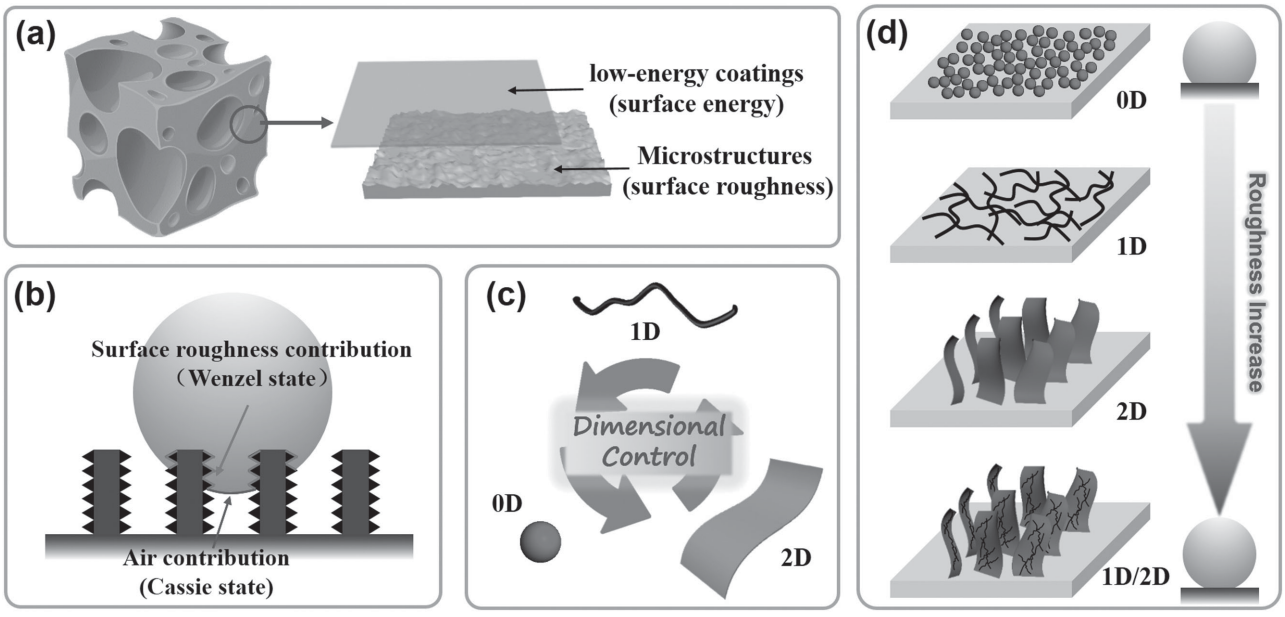

Figure 1. Schematic illustration of a) the structure of a 3D superhydrophobic foam, b) the contribution of the hydrophobic surface and trapped air pocket for superhydrophobicity, and c) the different dimensions of employed microstructures. d) The conceptual illustration of stepwise modulation of the wettability of materials by engineering the dimension of microstructures.

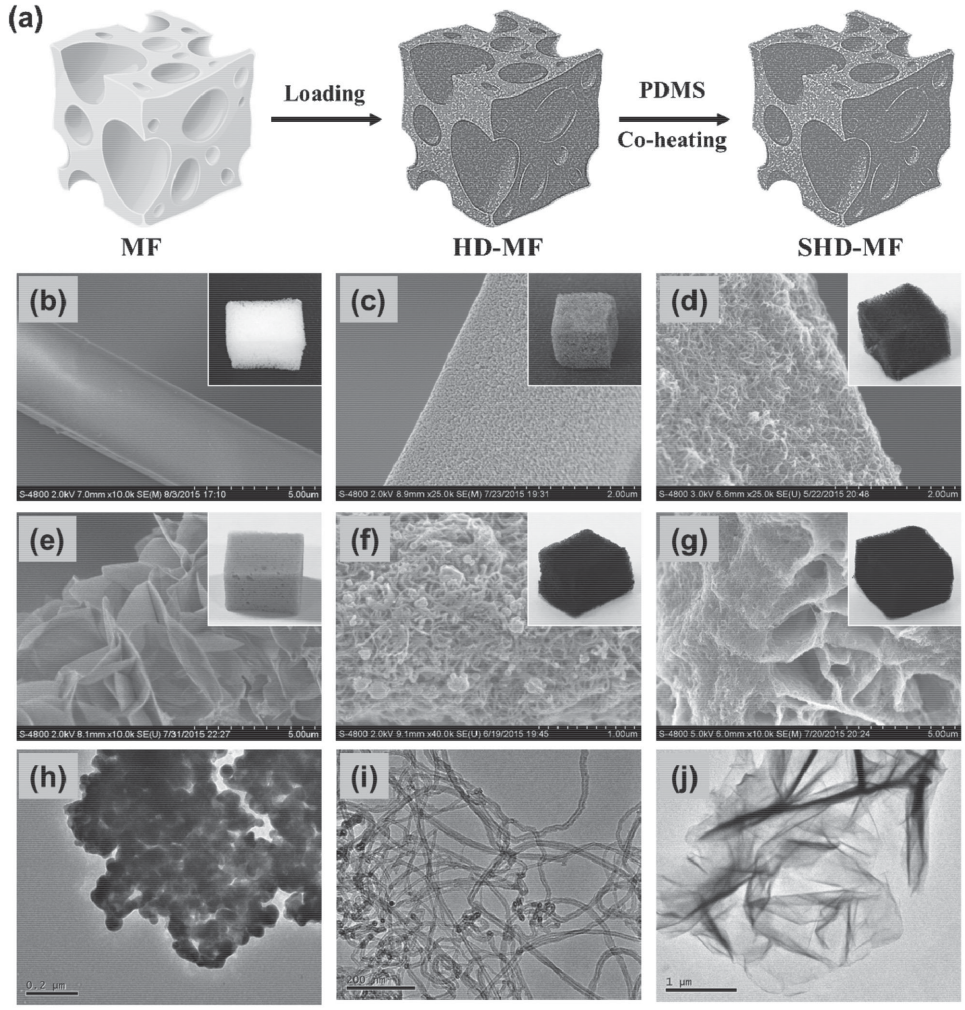

Figure 2. a) Schematic demonstration of the general synthetic route of superhydrophobic MF with hierarchical-dimension microstructures (SHD-MF). b–g) SEM images of pristine MF, MF-0D, MF-1D, MF-2D, MF-0/1D, and MF-1/2D, respectively. Insets are digital photos of corresponding materials. h–j) The TEM images of employed microstructures with 0D, 1D, and 2D dimensions, respectively.

achieve by other means such as graphene modification reported elsewhere.[37] The microstructures on MF-0D, MF-1D, and MF-2D were also examined by TEM (Figure 2h–j and Figure S5, Supporting Information), which confirmed three-type dimensions (0D, 1D, and 2D). To further expand the surface roughness range, more complex MF-0/1D and MF-1/2D were fabricated via a second-round loading process by using MF-1D and MF-2D as precursors, respectively. For MF-0/1D, 0D cobalt nanoparticles were randomly distributed on the as-existed 1D CNTs underlayer, contributing additional surface roughness. The most exciting thing is that for MF-1/2D, the loaded CNTs can conformally deposit on as-prepared $Co(OH)_2$ sheets of MF-2D, thus generating a novel microstructure of vertically aligned 1D nanotubes covered 2D sheets. This unique structure can significantly improve the R_f, since the apparent surface roughness for this structure is represented by the multiplication of R_f of 1D nanotubes and R_f of 2D sheets (see the Supporting Information), which dramatically expands the range of R_f.

After microstructures fabrication, a simple PDMS vapor deposition method[15,29] was used to create a conformal low-energy layer throughout the 3D networks of HD-MF, thus producing superhydrophobic HD-MF (denoted as SHD-MF). Corresponding SHD-MF with different microscopic dimensions are denoted as SMF-*X*D. The top PDMS coating can not only provide a hydrophobic surface from the aspect of chemical composition but also strengthens the adhesion of microstructures on the substrate and prevent them from direct contacting water. As shown in Figure S7 (Supporting Information), HD-MF can retain the original morphology after modification by PDMS, thereby allowing the further investigation of the relationship between microscopic dimensions and superhydrophobic properties of corresponding substrates (the numerical data are summarized in Table S1, Supporting Information). Herein, the used materials (e.g., CNTs, cobalt) for microstructures fabrication possess different chemical compositions. While the deposited PDMS conformal layer on surfaces can eliminate this difference, thus enabling investigation of pure effect of microstructures. On this basis, theoretically any material can be used to construct the microstructures regardless of their chemical compositions, which reflects the flexibility and universality of

our approach. Considering the potential adverse effect of CNTs and cobalt salt, the utilization of more eco-friendly materials for microstructures fabrication is preferred for practical use. Besides, the presented method is also scalable (Figure S8, Supporting Information), where the size of the products is only limited by the size of employed vessels or the original size of foams.

As displayed in **Figure 3**a, the contact angle can be readily tuned by changing the employed microscopic dimensions, ranging from 151.5° for SMF-0D to 163.2° for SMF-1/2D, which are much higher than that of PDMS-coated pristine MF (≈140°) and many other 3D hydrophobic substrates without such elaborate microstructure design.[29,35,36,38,40,43] To understand the underlying mechanism of microscopic dimensions directed hydrophobicity variation, theoretical models were established for each SHD-MF, and corresponding surface roughness on the foam (which is expressed by the actual area divided by the geometric projected area[4,50] were calculated ranging from 3.91 to 12.74 (Figures S9–S13, Supporting Information). It should be noted that the calculated surface roughness here is relative to the melamine foam. It was found that the static water contact angle was positively correlated to the surface roughness (Figure 3b), which seems consistent with Wenzel's prediction.[50] However, a careful observation revealed the deviation of derived curve (inset in Figure 3b) from the linear relationship given by Wenzel equation

$$\cos\theta_W = R_f \times \cos\theta_Y \quad (1)$$

where the θ_W and θ_Y represent the CA predicted by Wenzel's model (on the rough surface) and Young's model (on the flat surface), respectively. In Equation (1), θ_Y and R_f are determined by the chemical nature of surface coatings and the microstructure-induced surface roughness, respectively. Hence, with the same PDMS coating, all substrates should share the same θ_Y, thus leading to a linear relationship between R_f and obtained CA. Additionally, since the square of the normalized roughness

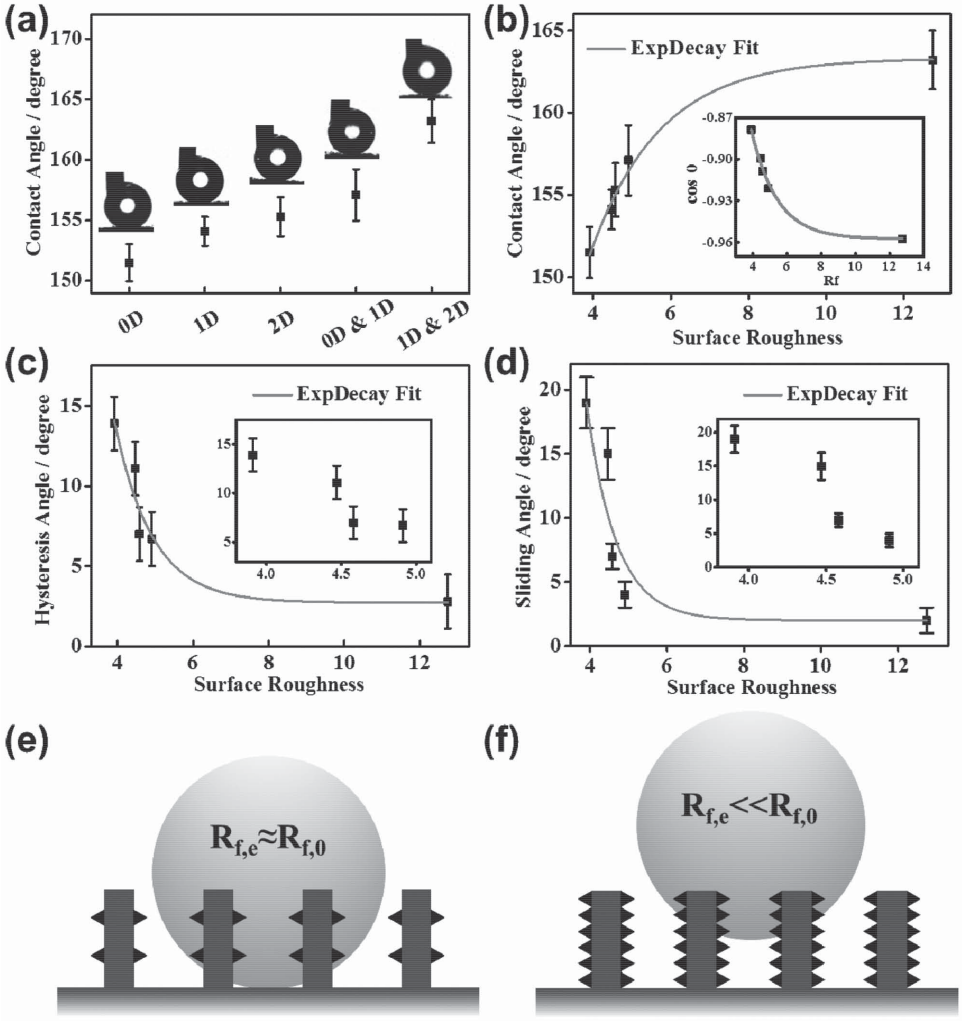

Figure 3. a) The plot of water CA versus SHD-MF with different microscopic dimensions. The plot of b) water CA, c) hysteresis angle, and d) sliding angle versus surface roughness on SHD-MF. Inset in (b) showed the plot of $\cos\theta$ versus R_f, while the inset in (c) and (d) showed the magnification diagram of low R_f region in corresponding figures. e,f) The schematic demonstration of the state of water droplet on rough surfaces. e) Water droplet possesses an effective roughness ($R_{f,e}$) close to the intrinsic surface roughness ($R_{f,0}$) on a less-roughness surface, but f) an $R_{f,e}$ much smaller than the $R_{f,0}$ on an extremely rough surface (see that the droplet can only feel a small fraction of the surface morphology).

size (l^2/V) in all of our SHD-MF is lower than 10^{-3} (l represented the half of the horizontal distance between two vertices, V represented the drop volume),[51] the Wenzel equation should be basically correct in our system. Thereby, the reason accounting for the deviation may arise from the coexistence of Wenzel state and Cassie state. By considering the hydrophobicity contributed by both the air and the solid surface, the apparent CA can be expressed as

$$\cos\theta_C = f_1 \times \cos\theta_W + (1 - f_1) \times \cos\theta_{air} \quad (2)$$

where the f_1, θ_{air} represent the fraction of the solid in contact with liquid, and the CA of liquid on the surface of air, respectively. Hence, the fraction of the solid in contact with air is $1 - f_1$.[4] It should be noted that unlike original Cassie–Baxter equation, herein the $\cos\theta_W$ rather than $\cos\theta_Y$ is used in the equation to depict the mixed Wenzel and Cassie state.[2,28] By substituting Equation (1) in Equation (2) and assuming the contact angle of water in air is 180°, then we have

$$\begin{aligned}\cos\theta_C &= f_1 \times R_f \times \cos\theta_Y + (1 - f_1) \times (-1) \\ &= f_1 \times R_f \times \cos\theta_Y + (f_1 - 1)\end{aligned} \quad (3)$$

In this equation, the first term ($f_1 \times R_f \times \cos\theta_Y$) and the second term ($f_1 - 1$) represent the contribution of Wenzel's state (originate from the enlarged solid surface area) and Cassie's state (originate from the trapped air pocket), respectively. With increasing R_f, the Laplace pressure on water droplet increased due to the enlarged contact area, thus preventing the penetration of the droplet and obtaining smaller f_1 (Figure 3e,f). In this way, the contribution of Cassie's state is increased with increasing R_f, thus significantly weakening the effect of R_f. On the other hand, since the water penetration is greatly suppressed with high R_f, the droplet can only feel a small part of surface roughness. In another word, the roughness that experienced by the droplet (defined as effective roughness, $R_{f,e}$) is much smaller than the actual roughness (denoted as $R_{f,0}$) of the substrate, which means the R_f is considerably screened on highly rough surfaces. Thereby, the $R_{f,e}$ rather than $R_{f,0}$ should be used in Equation (2),[2] which further reduces the effect of R_f of the substrate.

Apart from the static CA, the microscopic dimensions design can also influence other superhydrophobic properties (Figure 3c,d and Figures S14–S16, Supporting Information). The CA hysteresis and the sliding angle decreased with increasing R_f, deviating from the linear relationship like that of water CA. Intriguingly, substantially improved performance of water bouncing with increasing R_f was observed, where the water droplet showed 0, 1, and even 4 times bounce on SMF-0D (R_f = 3.91), SMF-2D (R_f = 4.61), and SMF-1/2D (R_f = 12.74), respectively. This might be attributed to the fact that the high water repellence on the high R_f substrate suppressed the energy dissipation of the water droplet during impacting with the foam, thus leading to the larger elastic collision fraction and facilitating more bouncing times. On a soft porous substrate, one time bounce is enough to show excellent superhydrophobicity,[41] so the power of microscopic dimensions engineering is evident from the four times bounce on SMF-1/2D. To sum up, by evaluating the superhydrophobic properties of different SHD-MF, it can be seen that the superhydrophobicity is positively correlated to the surface roughness. The overall improvement of superhydrophobicity, from the data of static CA, CA hysteresis, and sliding angle becomes less evident at high R_f (≈6–8). However, the water repellent nature represented by the water bouncing experiment, is continuously improved with increasing R_f in the whole range of measured surface roughness. It should be noted the surface roughness also closely depends on the size of specific microstructures. For example, with the same coverage, the CNTs with smaller diameters can give higher R_f than that of large-diameter CNTs. Hence, with diverse available microstructures, the theoretical modulation range of the hydrophobicity can be greatly widened by selecting well-defined structures with appropriate size. In another word, the presented concept can be used to devise versatile materials with desirable wettability in a controllable way.

The mechanical properties of materials are always important for their practical applications. As shown in Figure S17 (Supporting Information), the compression behaviors of those superhydrophobic foams were measured. Most SHD-MF inherited the excellent flexibility of melamine foams and possess a reversible compression strain up to 60%. Additionally, SMF-2D was further subjected to cycling test, where a plastic strain less than 5% was observed after 500th compression cycles, suggesting its good resistance to fatigue.

Finally, to test the potential of as-prepared SHD-MF for practical applications, SMF-2D was selected for its relatively simple synthetic route and high hydrophobicity. Since SMF-2D showed excellent superhydrophobicity and under-oil water repellency throughout the whole 3D network (**Figure 4**a,b and Figure S19, Supporting Information), one relevant application is the oil/water separation. The separation performance is evaluated by using a piece of SMF-2D (thickness ≈ 2.5 mm) as the filter and a mixture of 50 mL hexane/water (V/V: 4/1) as the test solution. During the whole separation process, the hexane (transparent) can continuously penetrate the filter while the water (purple color) was blocked. The separation ratio is higher than 99% calculated by our previous reported method,[36,45] suggesting the high performance of SMF-2D. Moreover, after usage, the SMF-2D can be easily regenerated by solvent (e.g., acetone) washing and drying, prolonging its life span. It should be noted the SMF-2D based filter is quite stable. Both the contact angle and morphology did not show obvious changes before and after separation cycles (Figure S18, Supporting Information).

The intrusion pressure (reflects the maximum height of the liquid that the filter can withstand) is an important parameter that determines the maximum processing capacity of a filter.[20,24] As analyzed above, a small water droplet showed the mixed Wenzel and Cassie state on the SMF-2D. However, with water accumulation during separation process, the increased static pressure ($p_s = \rho g h$) stemmed from increasing height of water column will inevitably induce the Cassie-to-Wenzel state transition.[1] Thus, the foam will be gradually wetted by water from the top to the bottom (along the z direction) with stepwise water penetration driven by p_s. Finally, the whole foam will be completely wetted and thus losing the separation ability. In our case, the measured intrusion pressure was ≈ 0.8 kPa, which is comparable to that of hydrophobic copper foams and porous nitrocellulose membranes.[20,24] Thanks to the flexibility and elasticity of SMF-2D inherited from pristine foam, the processing capacity can be easily increased by stacking several

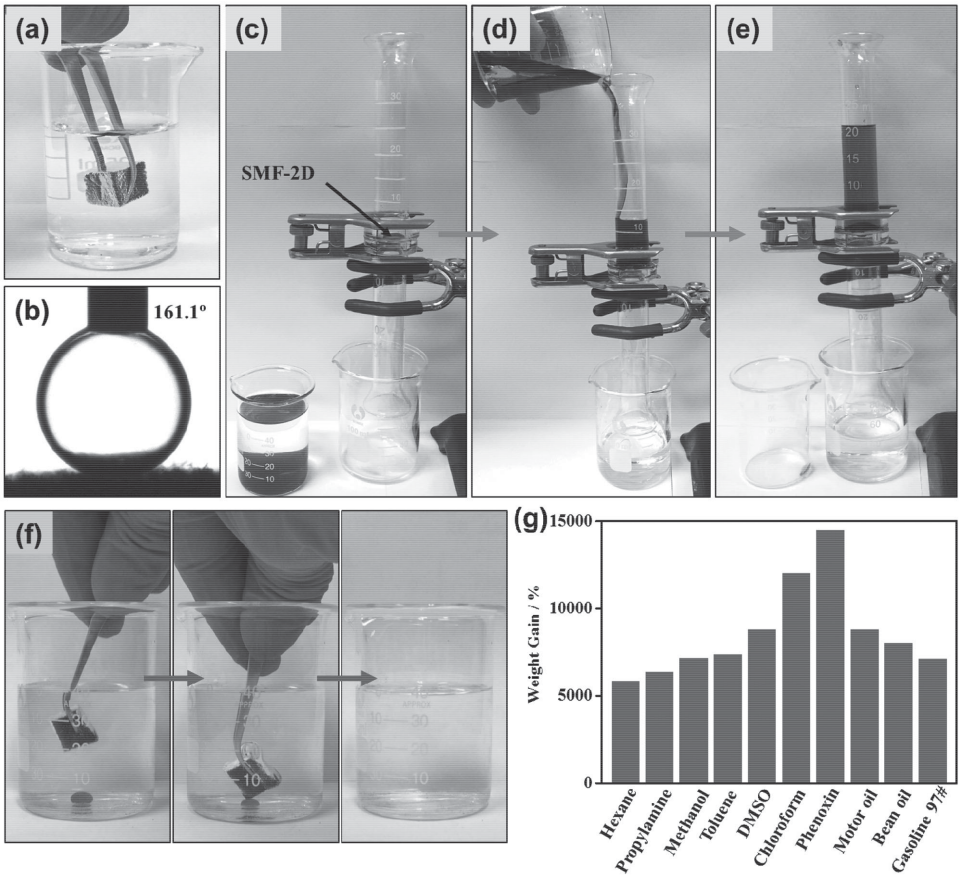

Figure 4. a) A piece of SMF-2D showed a silver color in water. b) The water CA of SMF-2D in the hexane. c–e) The digital photos of oil/water separation process by using SMF-2D as the filter. The water was stained with xylenol orange. f) Under-water adsorption of chloroform (dyed by Sudan III) by a piece of SMF-2D. g) The adsorption capacity of SMF-2D toward a variety of organic solvents and oils.

foams together, which equals to increasing the number of superhydrophobic surfaces along the *z* direction. In this way, theoretically the intrusion pressure and the processing capacity could be substantially increased.

The as-prepared foams can also be utilized to selectively remove oil from water because of its superhydrophobicity/superoleophilicity. As shown in Figure 4f, the underwater chloroform droplet was completely adsorbed by a piece of SMF-2D within a few seconds. The silver appearance of SMF-2D is attributed to the air/water around the foam, suggesting the remarkable hydrophobicity of SMF-2D.[29] Additionally, as illustrated in Figure 4g, the foam can adsorb a wide range of oils and organic solvents with high capacity (50–145 times weight gain), validating its great potential in water remediation.

To summarize, a new strategy of microscopic dimensions engineering was proposed to manipulate the surface wettability on 3D soft substrates. By combining wet and dry chemistry, a series of superhydrophobic melamine foams with different microscopic dimensions (0D, 1D, 2D, 0/1D, 1/2D) have been fabricated. Through both theoretically modeling and extensive experiments, the relationship between superhydrophobic performances (represent by static CA, CA hysteresis, sliding angle, and water bouncing) and the surface roughness is established, justifying the importance of high R_f on acquiring superior superhydrophobic materials. The derived relationship is valuable for devising materials with tailored wettability by modulating the surface roughness. Finally, SMF-2D was used as an example to show the power of microscopic dimensions engineering in oil/water separation and selective oil adsorption. We expected the presented microscopic dimensions design may serve as a new strategy to effectively engineer the 3D superhydrophobic substrate, and our results may shed light on devising desirable superwettable materials by appropriate surface roughness manipulation.

Supporting Information

Supporting Information is available from the Wiley Online Library or from the author.

Acknowledgements

This work was supported by NSFC (20903009, 50972001, 20725307, 51432002 and 50821061) and MOST (2011CB932601). Thank you for the language editing by Manish Kumar Priydarshi.

Received: September 15, 2015
Revised: October 24, 2015
Published online: November 30, 2015

[1] A. Lafuma, D. Quéré, *Nat. Mater.* **2003**, *2*, 457.
[2] A. Marmur, *Langmuir* **2003**, *19*, 8343.
[3] T. Darmanin, F. Guittard, *J. Mater. Chem. A* **2014**, *2*, 16319.
[4] Y. Tian, B. Su, L. Jiang, *Adv. Mater.* **2014**, *26*, 6872.
[5] L. Feng, Z. Zhang, Z. Mai, Y. Ma, B. Liu, L. Jiang, D. Zhu, *Angew. Chem., Int. Ed.* **2004**, *43*, 2012.
[6] Z. Xue, S. Wang, L. Lin, L. Chen, M. Liu, L. Feng, L. Jiang, *Adv. Mater.* **2011**, *23*, 4270.
[7] K. Li, J. Ju, Z. Xue, J. Ma, L. Feng, S. Gao, L. Jiang, *Nat. Commun.* **2013**, *4*, 2276.
[8] Y. Zhu, D. Wang, L. Jiang, J. Jin, *NPG Asia Mater.* **2014**, *6*, e101.
[9] Z. Chu, Y. Feng, S. Seeger, *Angew. Chem., Int. Ed.* **2015**, *54*, 2328.
[10] B. Wang, W. Liang, Z. Guo, W. Liu, *Chem. Soc. Rev.* **2015**, *44*, 336.
[11] R. Blossey, *Nat. Mater.* **2003**, *2*, 301.
[12] J. Bico, C. Marzolin, D. Quéré, *EPL* **1999**, *47*, 220.
[13] T. Sun, G. Wang, H. Liu, L. Feng, L. Jiang, D. Zhu, *J. Am. Chem. Soc.* **2003**, *125*, 14996.
[14] L. Jiang, Y. Zhao, J. Zhai, *Angew. Chem.* **2004**, *116*, 4438.
[15] J. Yuan, X. Liu, O. Akbulut, J. Hu, S. L. Suib, J. Kong, F. Stellacci, *Nat. Nanotechnol.* **2008**, *3*, 332.
[16] X. Deng, L. Mammen, H.-J. Butt, D. Vollmer, *Science* **2012**, *335*, 67.
[17] T. Verho, J. T. Korhonen, L. Sainiemi, V. Jokinen, C. Bower, K. Franze, S. Franssila, P. Andrew, O. Ikkala, R. H. Ras, *Proc. Natl. Acad. Sci. USA* **2012**, *109*, 10210.
[18] S. Pechook, N. Kornblum, B. Pokroy, *Adv. Funct. Mater.* **2013**, *23*, 4572.
[19] Y. Cai, L. Lin, Z. Xue, M. Liu, S. Wang, L. Jiang, *Adv. Funct. Mater.* **2014**, *24*, 809.
[20] X. Gao, L. P. Xu, Z. Xue, L. Feng, J. Peng, Y. Wen, S. Wang, X. Zhang, *Adv. Mater.* **2014**, *26*, 1771.
[21] X. Feng, J. Zhai, L. Jiang, *Angew. Chem., Int. Ed.* **2005**, *44*, 5115.
[22] L. Feng, S. Li, Y. Li, H. Li, L. Zhang, J. Zhai, Y. Song, B. Liu, L. Jiang, D. Zhu, *Adv. Mater.* **2002**, *14*, 1857.
[23] L. Gao, T. J. McCarthy, *Langmuir* **2006**, *22*, 2966.
[24] D. Zang, C. Wu, R. Zhu, W. Zhang, X. Yu, Y. Zhang, *Chem. Commun.* **2013**, *49*, 8410.
[25] W. Lee, M.-K. Jin, W.-C. Yoo, J.-K. Lee, *Langmuir* **2004**, *20*, 7665.
[26] W.-K. Lee, C. J. Engel, M. D. Huntington, J. Hu, T. W. Odom, *Nano Lett.* **2015**, *15*, 5624
[27] X. Gui, J. Wei, K. Wang, A. Cao, H. Zhu, Y. Jia, Q. Shu, D. Wu, *Adv. Mater.* **2010**, *22*, 617.
[28] E. Singh, Z. Chen, F. Houshmand, W. Ren, Y. Peles, H. M. Cheng, N. Koratkar, *Small* **2013**, *9*, 75.
[29] L. Chen, R. Du, J. Zhang, T. Yi, *J. Mater. Chem. A* **2015**, 3, 20547.
[30] R. Du, N. Zhang, J. H. Zhu, Y. Wang, C. Y. Xu, Y. Hu, N. N. Mao, H. Xu, W. J. Duan, L. Zhuang, L. T. Qu, Y. L. Hou, J. Zhang, *Small* **2015**, *11*, 3903.
[31] R. Du, Q. Zhao, N. Zhang, J. Zhang, *Small* **2015**, *11*, 3263.
[32] H. W. Liang, Q. F. Guan, L. F. Chen, Z. Zhu, W. J. Zhang, S. H. Yu, *Angew. Chem., Int. Ed.* **2012**, *51*, 5101.
[33] Z.-Y. Wu, C. Li, H.-W. Liang, J.-F. Chen, S.-H. Yu, *Angew. Chem., Int. Ed.* **2013**, *52*, 2925.
[34] H.-P. Cong, X.-C. Ren, P. Wang, S.-H. Yu, *ACS Nano* **2012**, *6*, 2693.
[35] R. Du, N. Zhang, H. Xu, N. Mao, W. Duan, J. Wang, Q. Zhao, Z. Liu, J. Zhang, *Adv. Mater.* **2014**, *26*, 8053.
[36] R. Du, Z. Zheng, N. Mao, N. Zhang, W. Hu, J. Zhang, *Adv. Sci.* **2015**, *2*, 1400006.
[37] D. D. Nguyen, N.-H. Tai, S.-B. Lee, W.-S. Kuo, *Energy Environ. Sci.* **2012**, *5*, 7908.
[38] N. Chen, Q. Pan, *ACS Nano* **2013**, *7*, 6875.
[39] B. Wang, J. Li, G. Wang, W. Liang, Y. Zhang, L. Shi, Z. Guo, W. Liu, *ACS Appl. Mater. Interfaces* **2013**, *5*, 1827.
[40] Y. Gao, Y. S. Zhou, W. Xiong, M. Wang, L. Fan, H. Rabiee-Golgir, L. Jiang, W. Hou, X. Huang, L. Jiang, *ACS Appl. Mater. Interfaces* **2014**, *6*, 5924.
[41] Y. Lu, S. Sathasivam, J. Song, W. Xu, C. J. Carmalt, I. P. Parkin, *J. Mater. Chem. A* **2014**, *2*, 12177.
[42] C. Ruan, K. Ai, X. Li, L. Lu, *Angew. Chem., Int. Ed.* **2014**, *53*, 5556.
[43] Y. Yang, Z. Liu, J. Huang, C. Wang, *J. Mater. Chem. A* **2015**, *3*, 5875.
[44] Y. Wang, Y. Shi, L. Pan, M. Yang, L. Peng, S. Zong, Y. Shi, G. Yu, *Nano Lett.* **2014**, *14*, 4803.
[45] X. Gao, J. Zhou, R. Du, Z. Xie, S. Deng, R. Liu, Z. Liu, J. Zhang, *Adv. Mater.* **2015**, DOI: 10.1002/adma.201504407.
[46] P. D. Petrov, G. L. Georgiev, *Chem. Commun.* **2011**, *47*, 5768.
[47] A. E. Gash, T. M. Tillotson, J. H. Satcher, J. F. Poco, L. W. Hrubesh, R. L. Simpson, *Chem. Mater.* **2001**, *13*, 999.
[48] J.-S. Girardon, A. Constant-Griboval, L. Gengembre, P. Chernavskii, A. Khodakov, *Catal. Today* **2005**, *106*, 161.
[49] J. G. Speight, *Lange's Handbook of Chemistry*, 16th ed., McGraw-Hill, New York **2005**.
[50] R. N. Wenzel, *Ind. Eng. Chem.* **1936**, *28*, 988.
[51] G. Wolansky, A. Marmur, *Colloids Surf., A* **1999**, *156*, 381.